



Full Paper

Hyperoside ameliorates diabetic nephropathy induced by STZ via targeting the miR-499–5p/APC axis

Jingbo Zhou, Shu Zhang, Xinyi Sun, Yan Lou, Jinjing Bao^{**}, Jiangyi Yu^{*}

Department of Endocrinology, Jiangsu Province Hospital of Chinese Medicine, Affiliated Hospital of Nanjing University of Chinese Medicine, Nanjing 210029, Jiangsu, China

ARTICLE INFO

Article history:

Received 25 September 2020

Received in revised form

14 December 2020

Accepted 9 February 2021

Available online 13 February 2021

Keywords:

Hyperoside

Diabetic nephropathy

miR-499–5p

APC

ABSTRACT

Diabetic nephropathy is a serious complication of diabetes. Hyperoside has been widely reported to ameliorate diabetes-associated disease. The current study is designed to explore the mechanism of hyperoside in diabetic nephropathy. In the present study, high glucose was used to treat podocytes. Diabetic nephropathy mice models were established by high-fat feeding followed by multiple low dose injections of streptozocin. Western blot analysis was conducted for detection of extracellular matrix accumulation, inflammatory response and cell apoptosis. We found out that hyperoside improved high glucose-induced cell injury. Additionally, hyperoside prevented mice with diabetic nephropathy from diabetic symptoms and renal dysfunction. Mechanistically, hyperoside inhibited the mRNA and protein expression of APC. MiR-499–5p was found to be an upstream negative mediator of APC, and hyperoside induced the upregulation of miR-499–5p. MiR-499–5p bound with the 3' untranslated region of APC to inhibit its expression. Finally, rescue assays revealed that the suppressive effects of miR-499–5p overexpression on renal dysfunction were rescued by upregulation of APC in mice with diabetic nephropathy. In conclusion, these findings indicated that hyperoside ameliorates diabetic nephropathy via targeting the miR-499–5p/APC axis, suggesting that hyperoside may offer a potential tactic for diabetic nephropathy treatment.

© 2021 The Authors. Production and hosting by Elsevier B.V. on behalf of Japanese Pharmacological Society. This is an open access article under the CC BY-NC-ND license (<http://creativecommons.org/licenses/by-nc-nd/4.0/>).

1. Introduction

Diabetic nephropathy (DN), a microvascular complication of diabetes, ranks the first in end-stage renal disease (ESRD).¹ Approximately 30% diabetic patients are diagnosed with renal complications.² Tubulointerstitial fibrosis, glomerular basement membrane thickening, and mesangial cell hypertrophy are observed in diabetic nephropathy renal tissues.³ The typical symptoms of diabetic nephropathy are proteinuria and progressive glomerular dysfunction, which have brought great troubles in the treatment of diabetic nephropathy.⁴ Although current clinical therapies can improve the symptoms of diabetic nephropathy and

postpone its progression to ESRD, diabetic nephropathy is difficult to be cured.⁵

Recently, more researchers have been attracted to the total flavonoids in the *Abelmoschus manihot* flower.⁶ The main ingredients in total flavonoids are hyperoside, isoquercetin, and quercetin 3'-glucoside.⁷ Particularly, hyperoside occupies the biggest proportion.⁷ Hyperoside (quercetin-3-O-galactoside; C₂₁H₂₀O₁₂; CAS: 482-36-0) has been reported to modulate the progression of several diseases.^{8–10} As an example, hyperoside plays anti-inflammatory and anti-arthritis roles in LPS-stimulated human fibroblast-like synoviocytes and collagen-treated mice.¹¹ Hyperoside suppresses the effects of oxidized low-density lipoprotein via the oxLDL/LOX-1/ERK pathway in vascular smooth muscle cells.¹² In recent years, hyperoside has been widely reported to regulate the progression of DN by modulating microRNA or targeting the AKT/mTOR pathway in mice.^{13–15}

MicroRNAs (miRNAs), a category of noncoding RNAs with 20–24 nucleotides in length, lack the capacity to encode proteins and frequently participate in the regulation of diseases.^{16,17} For example, miR-150–5p inhibits osteoarthritis development by

* Corresponding author. Jiangsu Province Hospital of Chinese Medicine, Affiliated Hospital of Nanjing University of Chinese Medicine, No. 155 Hanzhong Road, Nanjing, Jiangsu, China.

** Corresponding author.

E-mail address: yujiangyimed@sina.com (J. Yu).

Peer review under responsibility of Japanese Pharmacological Society.

targeting AKT3.¹⁸ In addition, miR-488–3p suppresses cardiomyocyte apoptosis in acute myocardial infarction via targeting ZNF791.¹⁹ Recently, miR-499–5p was reported to suppress C-reactive protein and exert a protective role in hypoxic-ischemic encephalopathy in rats.²⁰ Additionally, miR-499–5p can restrain cardiomyocytes injury induced by hypoxia/reoxygenation via targeting SOX6.²¹

MiRNAs have been revealed to target the wnt/ β -catenin signaling pathway in DN.^{22,23} Numerous studies indicated that the activation of Wnt/ β -catenin pathway contributes to the protection of kidney.^{24,25} According to genomic statistics, adenomatous polyposis coli (APC) gene, a negative regulator of the WNT signaling pathway, encodes a 312-kDa protein and performs various cellular functions.²⁶ APC acts as an inhibitive factor of the Wnt/ β -catenin signaling pathway by promoting phosphorylation, ubiquitination, and proteolytic degradation of β -catenin.²⁷ In the present research, we intended to figure out the function and mechanism of hyperoside in DN. We hypothesized that hyperoside may suppress APC levels to activate the Wnt/ β -catenin pathway. The upstream miRNAs for APC were also investigated. Our findings revealed that hyperoside ameliorated diabetic nephropathy induced by STZ via targeting the miR-499–5p/APC axis. This study may provide a potential tactic for DN treatment.

2. Materials and methods

2.1. Cell culture and cell treatment

The mouse podocytes were bought from the American Type Culture Collection (ATCC, Manassas, VA, USA) and cultivated in Dulbecco's modified Eagle medium (DMEM, Gibco, USA) added with 10% fetal bovine serum (FBS). High glucose (HG, 25 mmol/L) and normal glucose (5.5 mmol/L) were added into medium to establish *in vitro* model of diabetic nephropathy. The podocytes were cultured in a humidified atmosphere with 5% CO₂ at 37 °C. For drug administration, hyperoside (purity \geq 98%, Nanjing Zelang Medical Technological company, Nanjing, China) were dissolved in dimethyl sulfoxide (DMSO; Sigma–Aldrich, USA). Podocytes were treated with 2 mmol/L of hyperoside for 24 h, and control cells were treated with the same dose of DMSO (Sigma–Aldrich).

2.2. Cell transfection

The full length of APC was subcloned into the pcDNA3.1 vector to construct APC overexpression vector with the empty pcDNA3.1 vector as a control. MiR-499–5p mimics (miR-499–5p), anti-miR-499–5p and control vectors were purchased from GenePharma (Shanghai, China) and transfected into podocytes using Lipofectamine 2000 (Invitrogen, Carlsbad, CA, USA) following the manufacturer's instructions.

2.3. Western blot

Protein samples from cultured podocytes or mice tissues were obtained using RIPA lysis buffer (Beyotime, Beijing, China) and separated on 10% sodium dodecyl sulfate polyacrylamide gel electrophoresis. 5% defatted milk was added after samples were moved onto polyvinylidene fluoride membranes. Later, samples were cultivated with primary antibodies for collagen I (ab34710, Abcam, Cambridge, USA), collagen IV (ab34710, Abcam), fibronectin (ab2413, Abcam), TNF- α (ab1793, Abcam), MCP-1 (ab9669, Abcam), IL-1 β (ab106278, Abcam), Bax (ab32503, Abcam), Bcl-2 (ab32124, Abcam), APC (ab15270, Abcam) and GAPDH (ab8245, Abcam)

overnight at 4°C. Subsequently, secondary antibodies were added in the dark for 1 h. Finally, proteins were evaluated by an increased chemiluminescence detection system.

2.4. Enzyme-linked immunosorbent assay (ELISA)

Protein levels of TNF- α , MCP-1 and IL-1 β in cell supernatants of podocytes or mice's serum were detected by corresponding Enzyme-Linked Immunosorbent Assay Kits under manufacturer's instructions.

2.5. Caspase-3 activity assay

A caspase-3 Activity Assay Kit (Cell Signaling Technology, Danvers, USA) was used for the evaluation of caspase-3 activity. In brief, podocytes were lysed with 30 μ l of 1 \times PathScan^R Sandwich ELISA Lysis Buffer. Then, cell lysate of podocytes was mixed in the substrate solution and then incubated at 37°C in the dark. At last, the relative fluorescence was tested by a fluorescence plate reader.

2.6. Reverse-transcription quantitative polymerase chain reaction (RT-qPCR)

The extraction of total RNA from cells or mice tissues was performed using TRIzol reagent (Invitrogen). The extracted RNAs were reverse transcribed into cDNA using a PrimeScript[®] RT reagent Kit (Takara, Dalian, China). A SYBR-Green Real-time PCR Master Mix kit (Invitrogen) with the Applied Biosystems 7500 was used for RT-qPCR. U6 and GAPDH were used as controls for normalization of miRNA and mRNA expression, respectively. Through the 2^{- $\Delta\Delta$ Ct} method, the relative expression levels of target genes were calculated.

2.7. Diabetic nephropathy mouse model and AAV transduction

C57BL/6 Male mice (6–8 weeks, 20–25 g, n = 80) purchased from Shanghai Animal Laboratory Center were divided into 8 groups (n = 10 in each group). The animal grouping is as follows: (1) Sham; (2) DN; (3) DN + Hyperoside; (4) DN + Insulin; (5) Sham + Mock + vector; (6) DN + Mock + vector; (7) DN + miR-499–5p + vector; (8) DN + miR-499–5p + APC. All animal assays were operated under a protocol according to the Institutional Research Animal Care Committee of Jiangsu Province Hospital of Chinese Medicine, Affiliated Hospital of Nanjing University of Chinese Medicine (Jiangsu, China). The mice were fed with a high-fat diet (including 65.0% regular feed, 20% sucrose, 10% lard and 5% cholesterol). Six weeks later, STZ solution (dissolved in 0.1 mmol/L of citric acid buffer, pH 4.4, 30 mg/kg^{28,29}) was injected into the left lower abdominal cavity for 5 consecutive days to establish diabetic mice models. Sham-operated mice were treated with sodium citrate. For mice in DN group without any other treatment, after 8 weeks of STZ injection, mice developing diabetic nephropathy were sacrificed. Greater than 10-fold increase in albuminuria compared with controls for that strain at the same age and gender is used as the research criteria for validating a mouse model of diabetic nephropathy.³⁰ For mice in DN group receiving other treatments, after 4 weeks of STZ injection, mice started receiving hyperoside or AAV treatment. Hyperoside was suspended in 1% carboxymethyl cellulose for mice treatment. In detail, mice were treated with hyperoside (30 mg/kg,³¹ once every day) via intra-gastric administration for 4 weeks and were then sacrificed. AAV (serotype 9, Vigene Biosciences, Shanghai, China) was packaged, rinsed, and titrated for

injection. AAV9 (1×10^{12} copies) containing the control sequence, miR-499–5p or/and APC was injected through the left renal vein of mice as described previously.³² In some assays, mice were daily injected with insulin (1 IU/kg, Ultratard, Denmark). Four weeks after AAV injection, the mice were sacrificed, weighed, and renal tissues were resected for other assays. The glomeruli tissues of mice were harvested as described previously.³³ All animal assays were operated in line with approved Institutional Animal Care and Use Committee protocols.

2.8. Biochemistry analysis

Twenty-four-hours urine collection was performed using metabolic cages, and urine volume was determined. The mice urine samples were evaluated by a protein estimation kit (Nanjing Jiancheng Bioengineering Institute, Nanjing, China). Urine albumin was determined by an ELISA kit according to the manufacturer's instructions. Blood urea nitrogen was detected using the Cobas C-111 chemistry analyzer. Plasma creatinine in each group was detected as described previously using a direct colorimetric Jaffe method.³⁴ The blood glucose kit (Beijing Solarbio Science & Technology, Beijing, China) was applied to measure the blood glucose through a tail-vein blood sampling method. As described earlier,^{35–37} systolic blood pressure, heart rate and GFR were measured using an automatic tail-cuff system (Visitech-Systems, Apex, NC) and plasma kinetics of FITC-Sinistrin (Fresenius-Kabi, Linz, Austria).

2.9. Histology staining

Parts of kidney's extractions from mice were rapidly immobilized in PBS with 4% paraformaldehyde and maintained in the paraffin. The sections with 4 mm in thickness were used for Periodic Acid-Schiff (PAS) and Masson staining as described.³⁸ Glomerular area and mesangial expansion index were quantified using Image-Pro Plus 5.1 software (Media Cybernetics Inc, Bethesda, MD).

2.10. Luciferase reporter assay

The wild-type (Wt) and mutant (Mt) 3'UTR of APC sequences were inserted into the pGLO luciferase reporter plasmid (Promega) to create pGLO-APC-3'UTR-Wt and pGLO-APC-3'UTR-Mut plasmids. Then, the wild-type (Wt) and mutant pGLO-APC-3'UTR luciferase reporter plasmid were cotransfected with miR-499–5p mimics, anti-miR-499–5p or control vector into podocytes using Lipofectamine 2000. The Dual-Luciferase Reporter System (Promega) was used to test luciferase activities. All the vectors used in this assay were brought from GenePharma.

2.11. Statistical analysis

Data are showed as the means \pm standard deviation. Statistical analysis was progressed using the SPSS (Chicago, IL, USA) and GraphPad Prism 5 software (San Diego, CA). Experiments were performed three times. Significance of the variance between 2

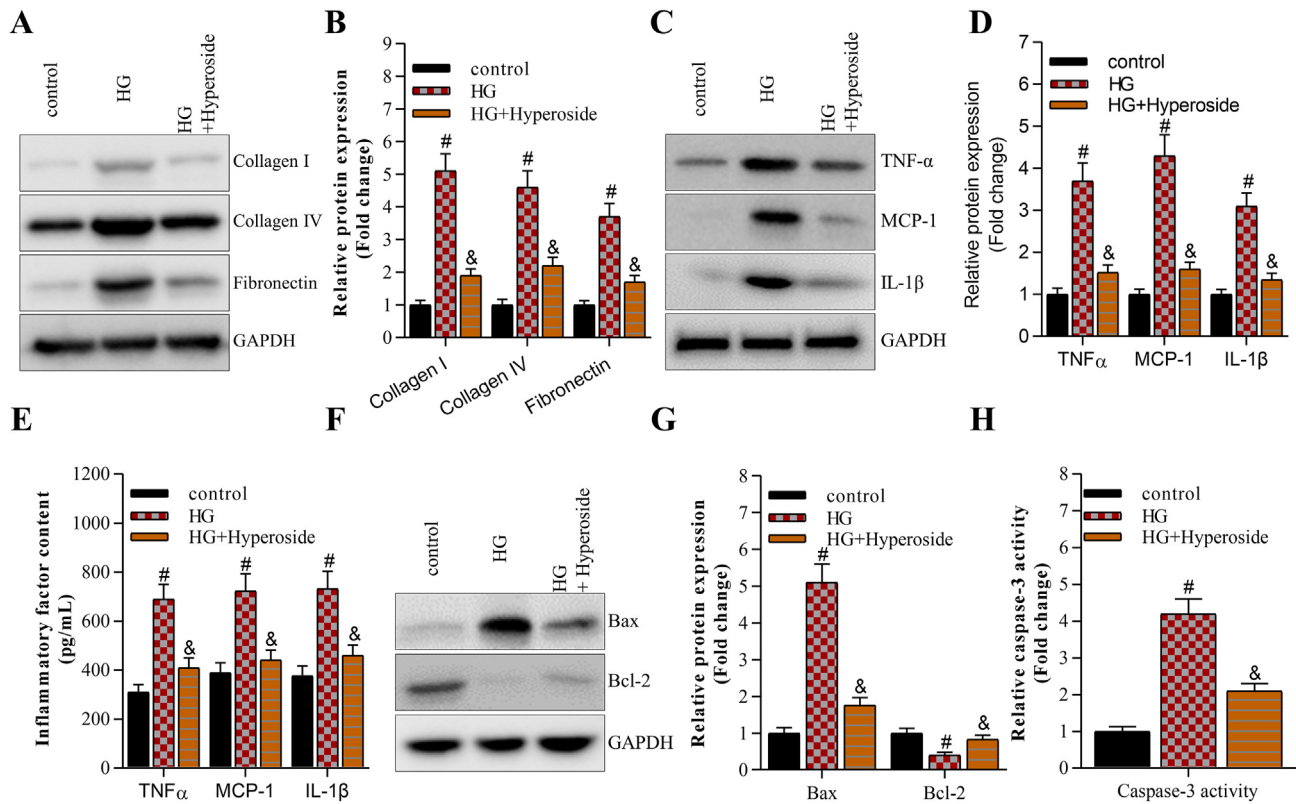


Fig. 1. Hyperoside inhibited high glucose-induced renal fibrosis, inflammation, and cell apoptosis in vitro. (A–D) Western blot analysis was used to measure collagen I, collagen IV, fibronectin, TNF- α , MCP-1, and IL-1 β protein levels in podocytes (E) ELISA was utilized to test contents of proinflammatory cytokines (TNF- α , MCP-1, and IL-1 β) in the supernatant of podocytes (F–G) The protein levels of Bax and Bcl-2 were detected by western blot in podocytes. (H) The test of caspase-3 activity in podocytes. Podocytes were treated with normal glucose, HG and/or hyperoside for 24 h #p < 0.05 VS. control group. &p < 0.05 VS. HG group.

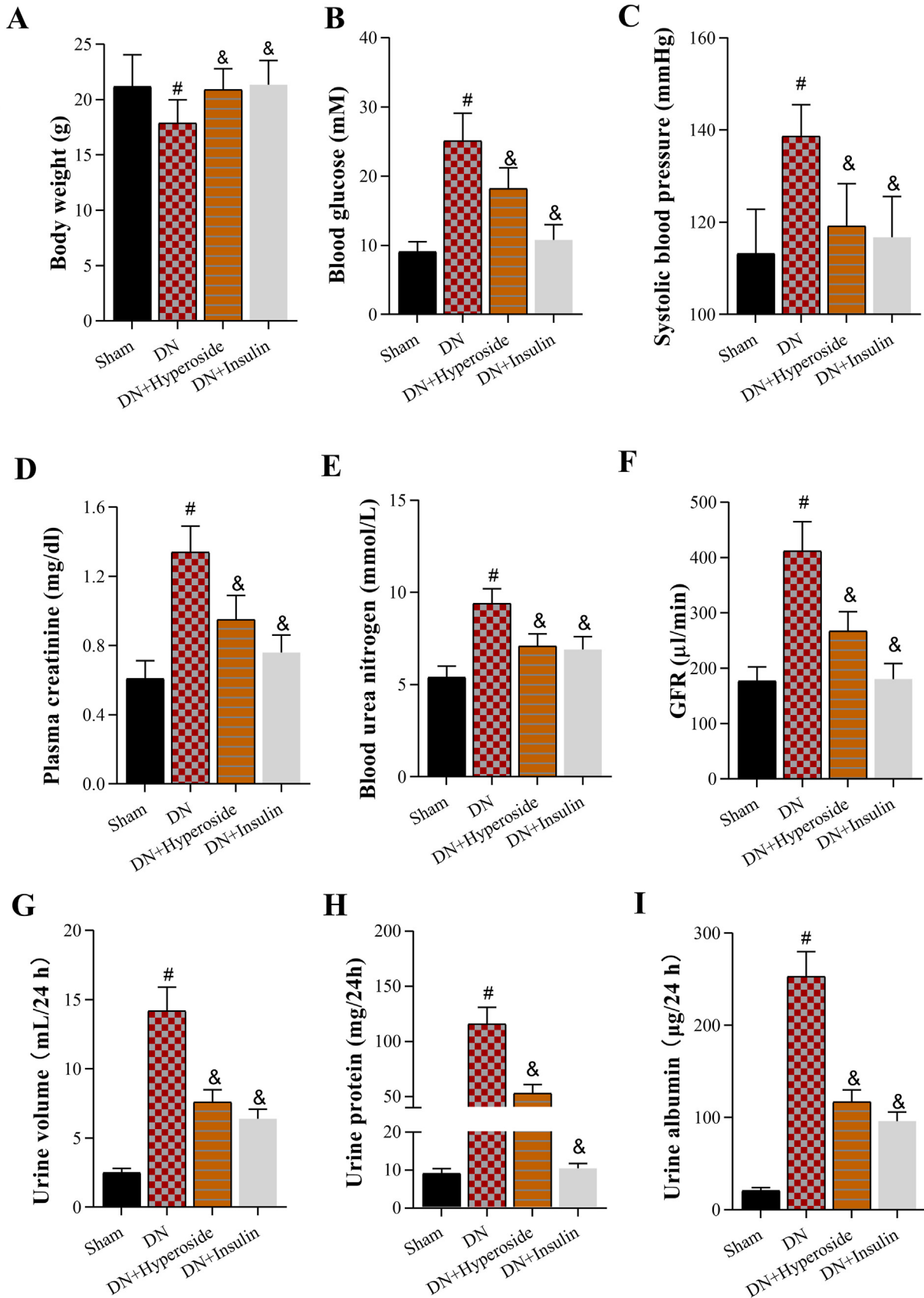


Fig. 2. Hyperoside alleviated diabetic symptoms of diabetic mice. (A–I) The examination of body weight, blood glucose, systolic blood pressure, plasma creatinine, blood urea nitrogen, GFR, urine volume, proteinuria, and urine albumin of mice in the different groups (n = 10 in each group). #p < 0.05 VS. Sham group. &p < 0.05 VS. DN group.

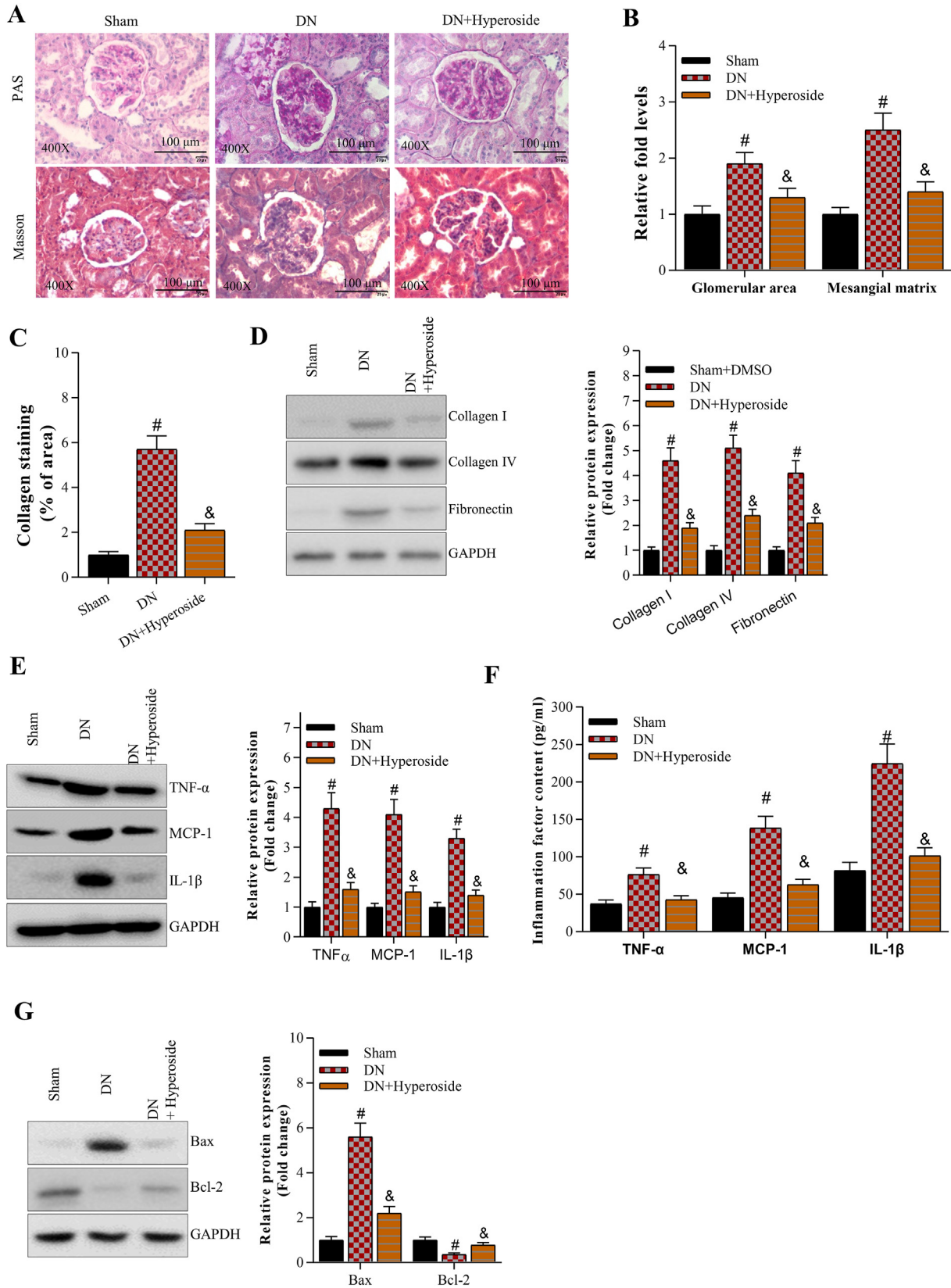


Fig. 3. MiR-499-5p alleviated diabetic nephropathy by targeting APC *in vivo*. (A) Histology immunostaining assay was used to observe the difference of renal histology between mice in control and DN model groups (n = 10 in each group) (B) The index of glomerular area and mesangial expansion in PAS-positive sections were determined (n = 10 in each group) (C) The collagen deposition in the glomerulus and renal interstitium was quantified (n = 10 in each group) (D–E) The protein levels of collagen I, collagen IV, fibronectin, TNF-α, MCP-1, and IL-1β in diabetic nephropathy mice models were detected by Western blot (n = 10 in each group) (F) The serum contents of cytokines (TNF-α, MCP-1, and IL-1β) were tested by ELISA in mice (n = 10 in each group) (G) The protein levels of Bax and Bcl-2 in diabetic nephropathy mice models were detected by Western blot (n = 10 in each group). #p < 0.05 VS. Sham group. &p < 0.05 VS. DN group.

groups was evaluated by Student's *t* tests and that among more than 2 groups was evaluated by analysis of variance. *P* < 0.05 had statistical significance.

3. Result

3.1. Hyperoside inhibited high glucose-induced extracellular matrix (ECM) accumulation, inflammation response and cell apoptosis *in vitro*

Hyperoside has been reported to alleviate chronic renal failure and renal fibrosis in mice,^{39–41} while the specific role of hyperoside in cellular processes in diabetic nephropathy remains unclear. Podocytes were treated with high glucose (25 mmol/L) to mimic cell injury with cells treated with normal glucose (5.5 mmol/L) as controls. According to Fig. 1A and B, levels of collagen I, collagen IV and fibronectin were significantly upregulated by high glucose, and then repressed by treatment of hyperoside. In addition, the protein levels of inflammatory cytokines including TNF- α , MCP-1 and IL-1 β were increased by high glucose. Meanwhile, hyperoside treatment rescued the proinflammatory effects of HG on podocytes (Fig. 1C–E). In addition, HG-induced the increase of Bax and the decline of Bcl-2 were countervailed by the treatment of hyperoside in podocytes (Fig. 1F and G). Finally, the caspase-3 activity was inhibited by HG treatment, and then reversed by hyperoside (Fig. 1H).

3.2. Hyperoside treatment improved diabetic symptoms of STZ-induced mice

To further explore the role of hyperoside *in vivo*, high-fat diet and STZ injection were used to induce diabetic nephropathy in mice. As

shown in Fig. 2A, the body weight was reduced in diabetic nephropathy mice, and then increased by hyperoside or insulin. In addition, the blood glucose, systolic pressure, plasma creatinine, blood urea nitrogen, GFR, urine volume, proteinuria, and albuminuria were elevated in mice with diabetic nephropathy, while the treatment of hyperoside or insulin reversed these results (Fig. 2B–I).

3.3. Hyperoside treatment mitigated renal injury and renal fibrosis of diabetic nephropathy mice

Based on the result of PAS and Masson's trichrome staining assay, we found out that hyperoside treatment counteracted the STZ-mediated increased area and size of glomerular (Fig. 3A). Moreover, STZ injection triggered significant increase of glomerular surface area and mesangial expansion in diabetic renal cortical sections along with abundant collagen accumulation in tubulointerstitial regions. However, such effects were alleviated by hyperoside treatment (Fig. 3B and C). Western blot analysis revealed that the accumulation of ECMs (collagen I, collagen IV and fibronectin) in renal tissues of diabetic nephropathy mice was alleviated by hyperoside treatment (Fig. 3D). Furthermore, Western blot and ELISA revealed that STZ-induced inflammatory response was inhibited by hyperoside treatment (Fig. 3E and F). At last, compared with Sham group, STZ-mediated the increase of Bax and the decrease of Bcl-2 protein levels were rescued by hyperoside treatment (Fig. 3G).

3.4. Hyperoside inhibited APC levels *in vitro* and *in vivo*

According to the results of RT-qPCR and western blot analyses, both mRNA and protein levels of APC were increased in podocytes in response to high glucose treatment, and then suppressed by

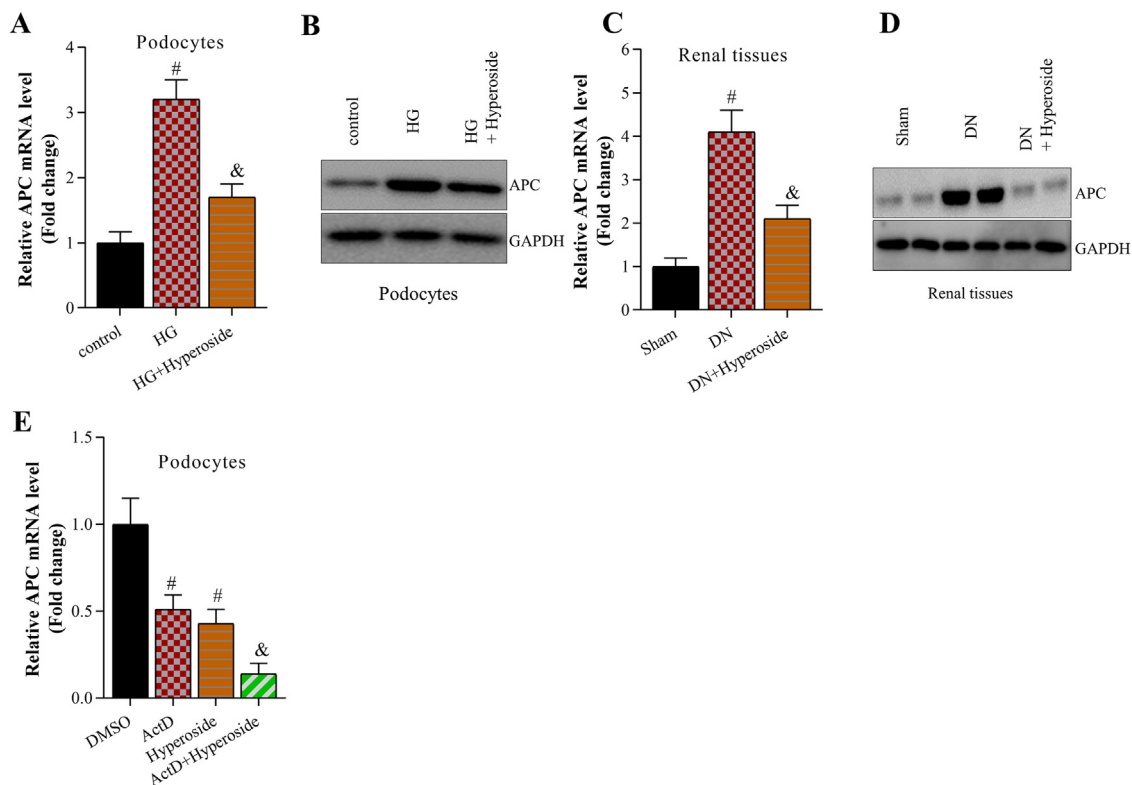


Fig. 4. Hyperoside inhibited APC levels *in vitro* and *in vivo*. (A–D) The examination of APC mRNA and protein levels was carried out in RT-qPCR and Western blot analyses in renal tissues (n = 10 in each group) and podocytes. [#]*p* < 0.05 VS. Sham or control group. [&]*p* < 0.05 VS. DN or HG group (E) The mRNA level of APC by Actinomycin D (an inhibitor of RNA enzyme) and/or hyperoside treatment was tested by RT-qPCR in podocytes. [#]*p* < 0.05 VS. DMSO group. [&]*p* < 0.05 VS. ActD group.

hyperoside addition (Fig. 4A and B). Likewise, STZ-induced the upregulation of APC protein levels in renal tissues were rescued by hyperoside treatment (Fig. 4C and D). Finally, either the treatment of ActD or hyperoside promoted the degradation of APC mRNA (Fig. 4E).

3.5. APC was directly targeted and negatively regulated by miR-499–5p

Previous studies proposed that miRNA can combine with the 3' untranslated region (3' UTR) of target mRNAs to modulate the levels of target mRNAs. Thus, we utilized Targetscan (<http://www.targetscan.org/>) database to predict potential miRNAs containing the binding site on the 3' UTR of APC. RT-qPCR analysis demonstrated that miR-499–5p displayed the most significant upregulation than other miRNAs in hyperoside-treated podocytes (Fig. 5A). Then, RT-qPCR revealed that miR-499–5p

levels were decreased in renal tissues of mice with diabetes nephropathy, and then increased by hyperoside treatment (Fig. 5B). Subsequently, the binding sequence between miR-499–5p and 3'UTR of APC was hypothesized by Targetscan and shown in Fig. 5C. Afterwards, the levels of miR-499–5p were respectively overexpressed and knocked down by transfection of miR-499–5p mimics and anti-miR-499–5p (Fig. 5D). In addition, luciferase reporter assay performed in podocytes illustrated that the luciferase activity of wild type pGLO-APC-3'UTR was significantly decreased by miR-499–5p overexpression, and increased by silencing of miR-499–5p. No significant alteration has been noticed in luciferase activity of mutant pGLO-APC-3'UTR (Fig. 5E). RT-qPCR and Western blot analyses revealed that both mRNA and protein levels of APC were increased by miR-499–5p overexpression, and decreased by miR-499–5p suppression (Fig. 5F). At last, miR-499–5p inhibition rescued the suppressive impact of hyperoside on APC mRNA level in podocytes (Fig. 5G).

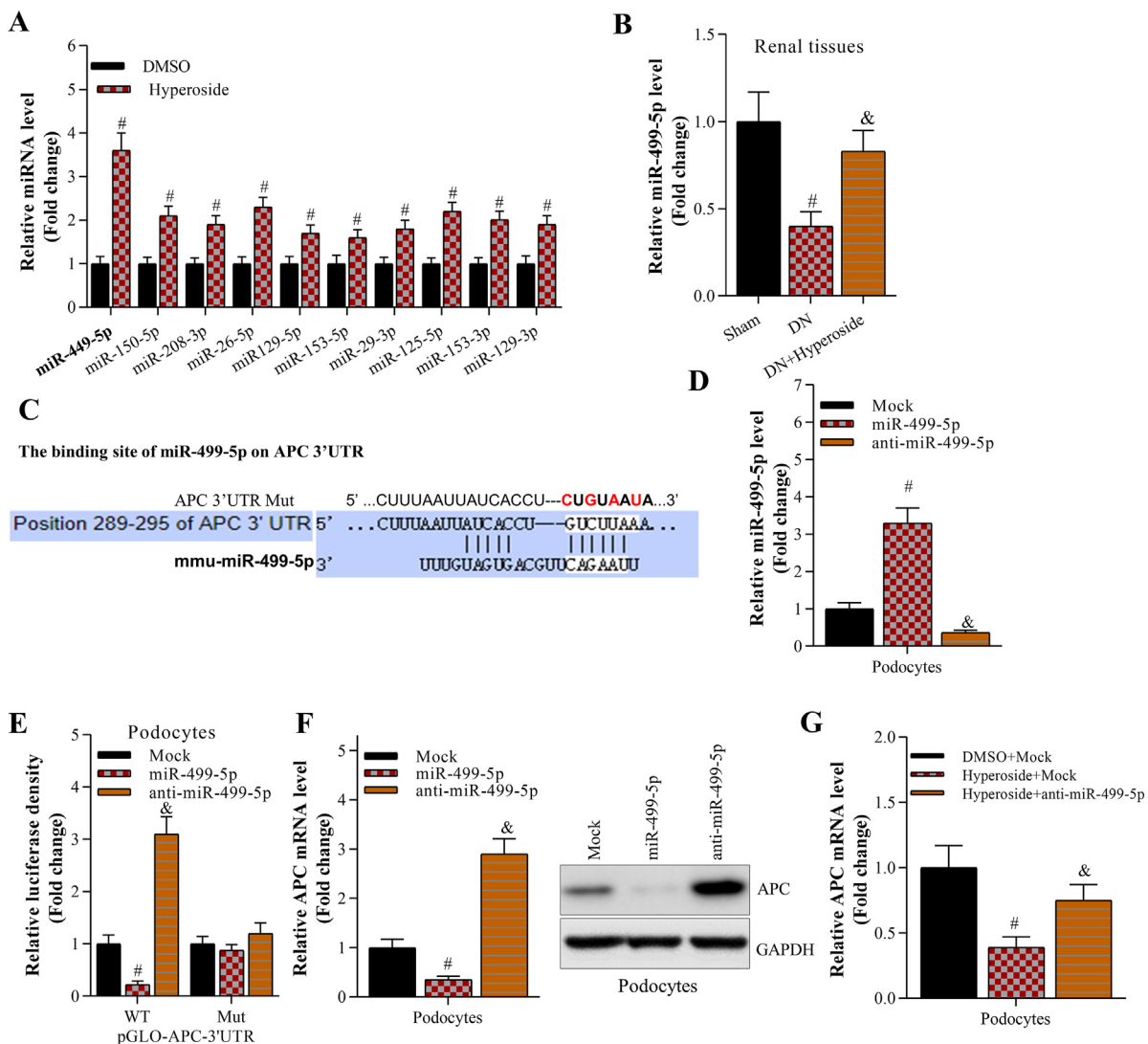


Fig. 5. APC was directly targeted and negatively regulated by miR-499–5p. (A) The potential miRNAs levels were determined by RT-qPCR in HG-treated podocytes. #p < 0.05 VS. DMSO group (B) The level of miR-499–5p in renal tissues (n = 10 in each group) of mice was measured by RT-qPCR. #p < 0.05 VS. Sham group. &p < 0.05 VS. DN group (C) The binding sites of miR-499–5p on APC 3'UTR were predicted by targetScan (D) The overexpression efficacy of miR-499–5p was evaluated by RT-qPCR. #p < 0.05 VS. Mock group. &p < 0.05 VS. Mock group (E) Luciferase reporter assay was used to confirm the binding capacity between miR-499–5p and APC 3'UTR. #p < 0.05 VS. Mock group. &p < 0.05 VS. Mock group (F) The measurement of APC mRNA and protein levels in podocytes were implemented by RT-qPCR and Western blot assays. #p < 0.05 VS. Mock group. &p < 0.05 VS. Mock group (G) The APC level in podocytes in different groups was monitored by RT-qPCR. #p < 0.05 VS. DMSO + Mock group. &p < 0.05 VS. Hyperoside + Mock group.

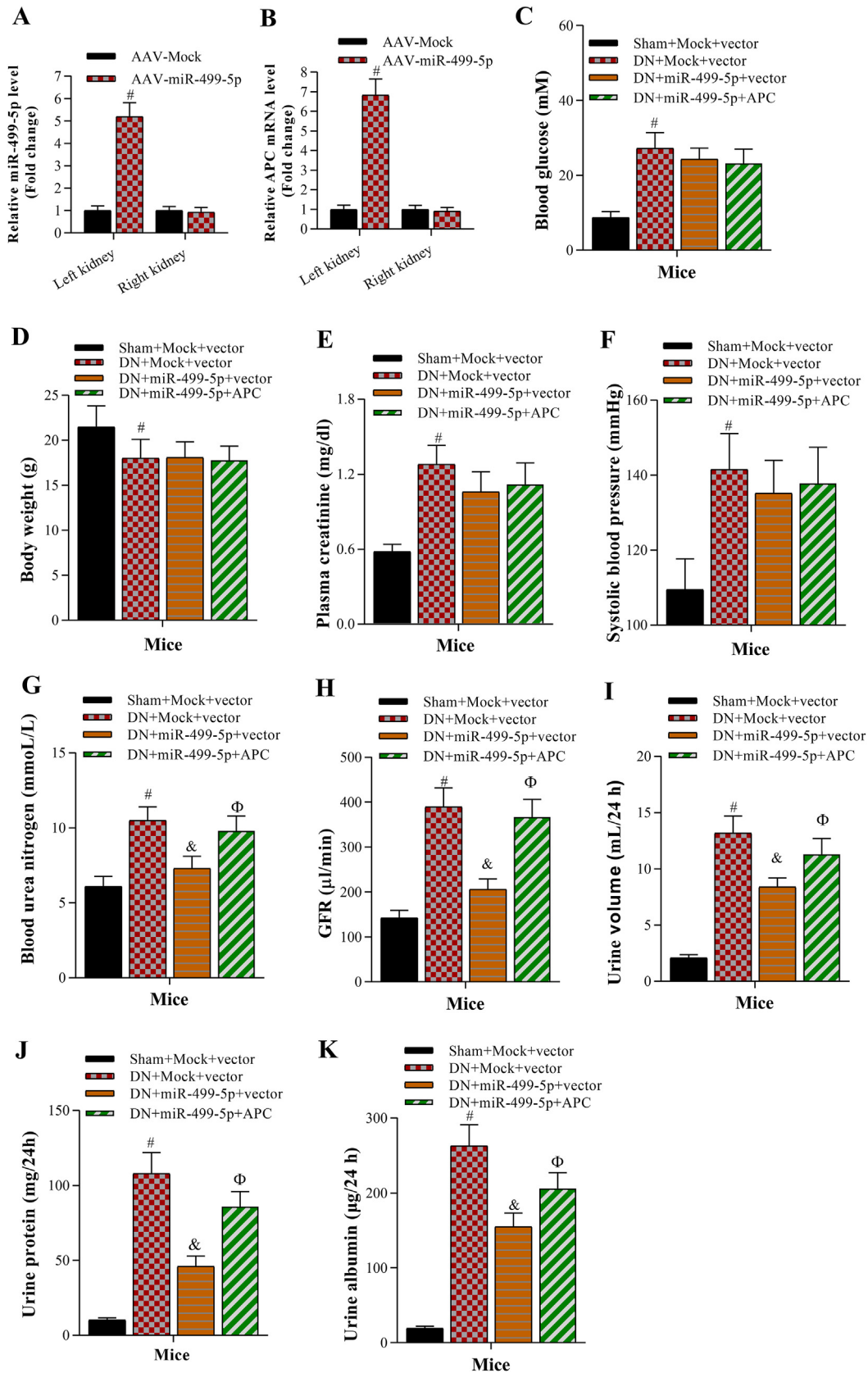


Fig. 6. MiR-499-5p and APC had no influence on diabetic symptoms of mice. (A–B) The examination of miR-499-5p and APC levels was conducted in RT-qPCR. #p < 0.05 VS. AAV-Mock group (n = 10 in each group) (C) The assessment of the effects of miR-499-5p and APC on blood glucose of mice (n = 10 in each group) (D–K) The examination of body weight, plasma creatinine, systolic blood pressure, blood urea nitrogen, GFR, urine volume, urine protein and albuminuria of mice in indicated groups (n = 10 in each group). #p < 0.05 VS. Sham + Mock + vector group. &p < 0.05 VS. DN + Mock + vector group. Φ p < 0.05 VS. DN + miR-499-5p + vector group.

3.6. **miR-499-5p and APC had no influence on diabetic symptoms of mice**

The levels of miR-499-5p and APC in left kidney tissues were significantly increased by injection of AAV-miR-499-5p and AAV-APC respectively, and no significant difference was observed in right kidney tissues (Fig. 6A and B). Moreover, neither miR-499-5p overexpression nor APC overexpression had effects on blood glucose, body weight, plasma creatinine, blood pressure of diabetic nephropathy mice (Fig. 6C–F). Finally, the suppressive impacts of miR-499-5p on blood urea nitrogen, GFR, urine volume, urine protein, and albuminuria were neutralized by APC overexpression (Fig. 6G–K).

3.7. **Overexpression of APC reversed the effect of miR-499-5p on renal injury and fibrosis**

Compared with DN + Mock + vector group, glomerular hypertrophy and glomerular surface area were reduced by injection of AAV-miR-499-5p. However, such influence was rescued by APC overexpression (Fig. 7A). Similarly, in diabetic nephropathy mice, the inhibitory influence of miR-499-5p on the glomerular surface area and mesangial extension, along with the collagen accumulation in tubulointerstitial areas were recovered by AAV-APC treatment (Fig. 7B and C). Similarly, the western blot analysis revealed that the decrease of ECM in renal tissues resulting from miR-499-5p was also counteracted by APC overexpression (Fig. 7D).

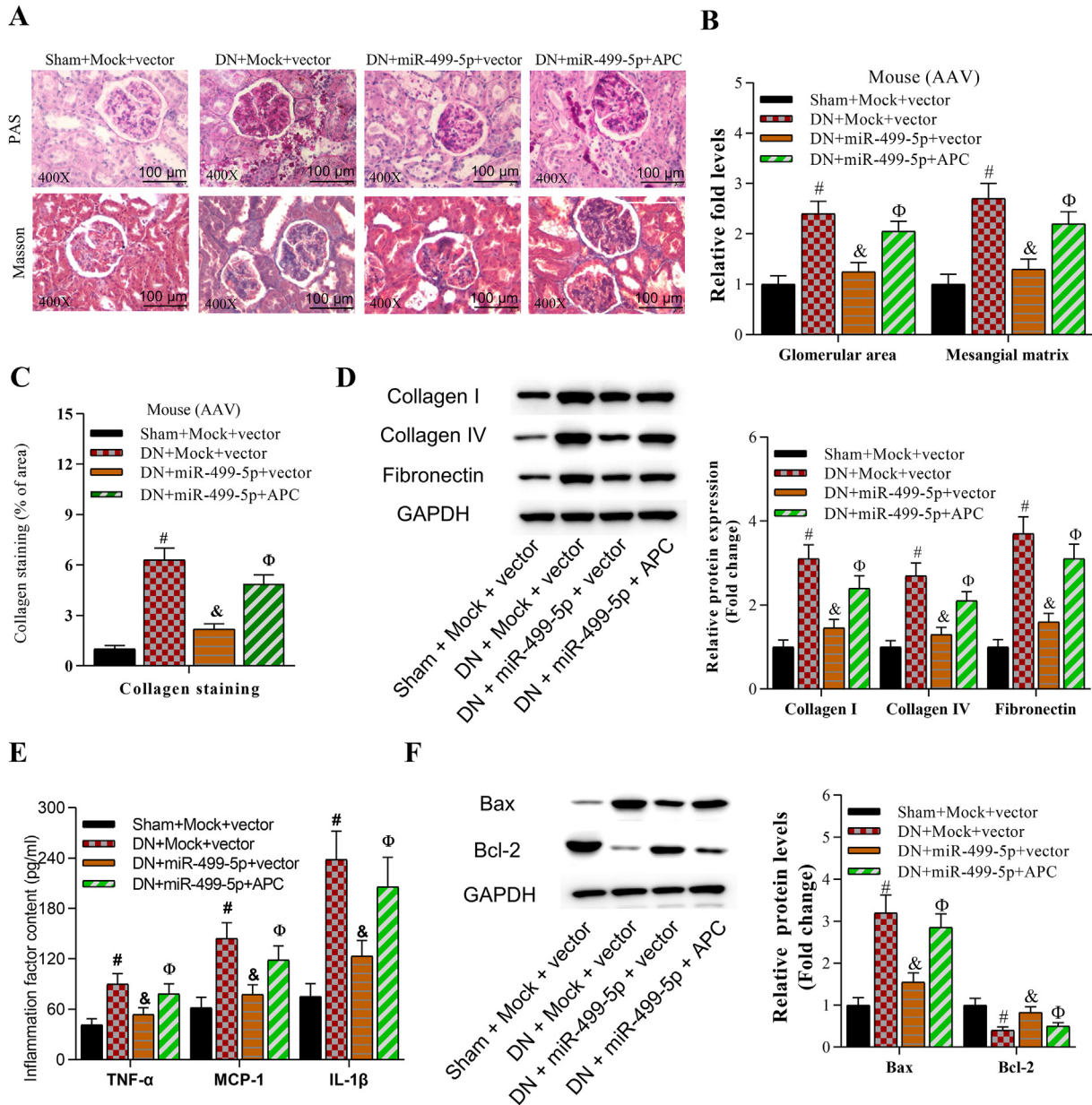


Fig. 7. Overexpression of APC reversed the effect of miR-499-5p on renal injury and fibrosis. (A) Histology immunostaining assay was performed to observe the structure of renal tissues (n = 10 in each group) (B) The index of glomerular area and mesangial expansion in PAS-positive sections from mice were determined (n = 10 in each group). [#]p < 0.05 VS. Sham + Mock + vector group. [&]p < 0.05 VS. DN + Mock + vector group. ^Φp < 0.05 VS. DN + miR-499-5p + vector group (C) The collagen deposition in the glomerulus and renal interstitium from mice was quantified (n = 10 in each group). [#]p < 0.05 VS. Sham + Mock + vector group. [&]p < 0.05 VS. DN + Mock + vector group. ^Φp < 0.05 VS. DN + miR-499-5p + vector group (D) The protein levels of collagen I, collagen IV and fibronectin, were studied by Western blot in indicated groups (n = 10 in each group) (E) The content of cytokines (TNF- α , MCP-1, IL-1 β) was examined by ELISA in indicated groups (n = 10 in each group) (F) The protein levels of Bax and Bcl-2 were assessed by Western blot in indicated groups (n = 10 in each group). [#]p < 0.05 VS. Sham + Mock + vector group. [&]p < 0.05 VS. DN + Mock + vector group. ^Φp < 0.05 VS. DN + miR-499-5p + vector group.

Furthermore, the contents of inflammatory cytokines were reduced by injection of AAV-miR-499–5p in serum of diabetic nephropathy mice. However, the result was counterbalanced by APC overexpression (Fig. 7E). The decrease of Bax and the increase of Bcl-2 proteins induced by AAV-miR-499–5p injection were rescued by APC overexpression in renal tissues of diabetic nephropathy mice (Fig. 7F).

4. Discussion

Diabetic nephropathy refers to diabetic glomerulosclerosis, a glomerular lesion with vascular damage.⁴² Known factors including metabolic disorders, glomerular hemodynamic alteration and genetic factors are closely associated with the incidence of diabetic nephropathy.⁴³ Several therapies like continuous ambulatory peritoneal dialysis and kidney transplant are employed to treat diabetic nephropathy, but the overall survival rates of patients with diabetic nephropathy remain low with dismal prognosis due to the immunological rejection after organ transplant.^{44,45} According to previous studies, the combination usage of high fat food and STZ injection were widely applied to mimic diabetic nephropathy *in vivo*.^{46,47} In the current study, we used these operations to induce diabetic nephropathy, and discovered that STZ treatment significantly induced histological changes and dysfunctions of mice kidneys. Additionally, collagen accumulation, inflammatory response and cell apoptosis in kidney tissues were induced by STZ.

Increasing studies revealed that some antidiabetic drugs like sodium/glucose cotransporter 2 inhibitors or glucagone-like peptide-1 agonists are effective to reduce blood glucose and alleviate DN. However, these drugs have side effects.^{48,49} Hence, to identify more potential effective drugs is necessary. Hyperoside exerts antihypoglycemic and hepatocyte-protective effects in diabetic mice.⁵⁰ Hyperoside can alleviate renal injury.^{51,52} Hyperoside alleviates glomerulosclerosis in diabetic nephropathy by downregulation of miR-21 to suppress Fibronectin and collagen IV expression as well as to promote MMP-9 and MMP-2 expression.¹³ Lei Zhou *et al.* revealed that pretreatment of hyperoside prevents renal damage and podocyte apoptosis in mice with diabetic nephropathy.¹⁴ Compared with previous studies, we discovered that hyperoside alleviated high glucose-induced podocyte injury not only by suppressing ECM deposition, cell apoptosis, but also by inhibiting inflammatory response in a miR-499–5p dependent way. Additionally, hyperoside can prevent mice with diabetic nephropathy from diabetic symptoms and renal dysfunctions.

Mechanistically, hyperoside can mediate microRNAs to regulate downstream target mRNAs. For instance, hyperoside serves as a potential therapeutic strategy for diabetic nephropathy by inhibition on miR-34a and CREB expression.⁵³ Hyperoside improves glomerulosclerosis by interacting with miR-21 and targeting MMP-9 in diabetic nephropathy.¹³ In our study, we found that hyperoside triggered significant decrease in APC mRNA and protein levels. Subsequently, miR-499–5p was identified as the upstream factor of APC.

We found that miR-499–5p can specifically bind with the 3'UTR of APC and negatively regulate APC expression. MiR-499–5p was downregulated in mice with diabetic nephropathy and inhibited apoptosis, inflammation, and collagen accumulation in kidney tissues. Previously, miR-499–5p expression was reported to be decreased in the livers of diabetic mice.⁵⁴ MiR-499–5p expression is reduced in erythrocytes of African American pre-diabetic patients⁵⁵ and in patients with diabetic nephropathy.⁵⁶ Expression of miR-499–5p is downregulated in patients with diabetic end-stage renal disease.⁵⁷ MiR-499–5p alleviates podocyte injury by calcineurin in minimal change disease.⁵⁸ MiR-499–5p promotes inflammation to aggravate nonalcoholic fatty liver disease.⁵⁹

Moreover, miR-499–5p is predicted to be involved in the Wnt/ β -catenin pathway.^{60,61} In our study, miR-499–5p inhibits the expression of APC, indicating that miR-499–5p potentially activates the Wnt/ β -catenin pathway. The inhibitory effects of miR-499–5p overexpression on renal injury were rescued by upregulation of APC in mice with diabetic nephropathy.

In conclusion, hyperoside ameliorates renal dysfunctions of mice with diabetic nephropathy and suppresses extracellular matrix accumulation, inflammatory response, and apoptosis of high glucose treated podocytes via the miR-499–5p/APC axis (Supplementary Figure). However, the function and mechanism of hyperoside has not been explored in clinical samples, and more mechanisms of hyperoside in diabetic nephropathy remain to be explored in the future.

Declaration of competing interest

The authors declare that there are no competing interests in this study.

Acknowledgement

We appreciate the support of Jiangsu Province Hospital of Chinese Medicine, Affiliated Hospital of Nanjing University of Chinese Medicine.

Funding

This work was supported by Jiangsu Provincial Hospital of Traditional Chinese Medicine (No. Y2019CX36).

Data availability statement

The datasets used during the current study are available from the corresponding author on reasonable request.

Appendix A. Supplementary data

Supplementary data to this article can be found online at <https://doi.org/10.1016/j.jphs.2021.02.005>.

References

1. Tziomalos K, Athyros VG. Diabetic nephropathy: new risk factors and improvements in diagnosis. The review of diabetic studies. *Reg Dev Stud*. 2015;12(1–2):110–118.
2. Haneda M, Utsunomiya K, Koya D, et al. A new classification of diabetic nephropathy 2014: a report from joint committee on diabetic nephropathy. *Clin Exp Nephrol*. 2015;19(1):1–5.
3. Wada J, Makino H. Inflammation and the pathogenesis of diabetic nephropathy. *Clin Sci (Lond)*. 2013;124(3):139–152.
4. Qi H, Casalena G, Shi S, et al. Glomerular endothelial mitochondrial dysfunction is essential and characteristic of diabetic kidney disease susceptibility. *Diabetes*. 2017;66(3):763–778.
5. Gross JL, de Azevedo MJ, Silveiro SP, Canani LH, Caramori ML, Zelmanovitz T. Diabetic nephropathy: diagnosis, prevention, and treatment. *Diabetes Care*. 2005;28(1):164–176.
6. Xue C, Guo J, Qian D, et al. Identification of the potential active components of *Abelmoschus manihot* in rat blood and kidney tissue by microdialysis combined with ultra-performance liquid chromatography/quadrupole time-of-flight mass spectrometry. *J Chromatogr B, Anal Technol Biomed Life Sci*. 2011;879(5–6):317–325.
7. Wu LL, Yang XB, Huang ZM, Liu HZ, Wu GX. In vivo and in vitro antiviral activity of hyperoside extracted from *Abelmoschus manihot* (L) mediak. *Acta Pharmacol Sin*. 2007;28(3):404–409.
8. He F, Li D, Wang D, Deng M. Extraction and purification of quercitrin, hyperoside, rutin, and afzelin from *Zanthoxylum bungeanum maxim* leaves using an aqueous two-phase system. *J Food Sci*. 2016;81(7):C1593–C1602.
9. Sun Y, Sun F, Feng W, et al. Hyperoside inhibits biofilm formation of *Pseudomonas aeruginosa*. *Exp Therapeut Med*. 2017;14(2):1647–1652.

10. Zou L, Chen S, Li L, Wu T. The protective effect of hyperoside on carbon tetrachloride-induced chronic liver fibrosis in mice via upregulation of Nrf 2. *Exp Toxicol Pathol : off J Gesellschaft fur Toxikologische Pathologie*. 2017;69(7):451–460.
11. Jin XN, Yan EZ, Wang HM, et al. Hyperoside exerts anti-inflammatory and anti-arthritis effects in LPS-stimulated human fibroblast-like synoviocytes in vitro and in mice with collagen-induced arthritis. *Acta Pharmacol Sin*. 2016;37(5):674–686.
12. Zhang Z, Zhang D, Du B, Chen Z. Hyperoside inhibits the effects induced by oxidized low-density lipoprotein in vascular smooth muscle cells via oxLDL-LOX-1-ERK pathway. *Mol Cell Biochem*. 2017;433(1–2):169–176.
13. Zhang L, He S, Yang F, et al. Hyperoside ameliorates glomerulosclerosis in diabetic nephropathy by downregulating miR-21. *Can J Physiol Pharmacol*. 2016;94(12):1249–1256.
14. Zhou L, An XF, Teng SC, et al. Pretreatment with the total flavone glycosides of *Flos Abelmoschus manihot* and hyperoside prevents glomerular podocyte apoptosis in streptozotocin-induced diabetic nephropathy. *J Med Food*. 2012;15(5):461–468.
15. Wu W, Hu W, Han WB, et al. Inhibition of akt/mTOR/p70S6K signaling activity with huangkui capsule alleviates the early glomerular pathological changes in diabetic nephropathy. *Front Pharmacol*. 2018;9:443.
16. Ruppaimoole R, Slack FJ. MicroRNA therapeutics: towards a new era for the management of cancer and other diseases. *Nat Rev Drug Discov*. 2017;16(3):203–222.
17. Vishnoi A, Rani S. MiRNA biogenesis and regulation of diseases: an overview. *Methods Mol Biol*. 2017;1509:1–10.
18. Zhang Y, Wang F, Chen G, He R, Yang L. LncRNA MALAT1 promotes osteoarthritis by modulating miR-150-5p/AKT3 axis. *Cell Biosci*. 2019;9:54.
19. Zheng HF, Sun J, Zou ZY, Zhang Y, Hou GY. MiRNA-488-3p suppresses acute myocardial infarction-induced cardiomyocyte apoptosis via targeting ZNF791. *Eur Rev Med Pharmacol Sci*. 2019;23(11):4932–4939.
20. Gu L, Shigemasa K, Ohama K. Increased expression of IGF II mRNA-binding protein 1 mRNA is associated with an advanced clinical stage and poor prognosis in patients with ovarian cancer. *Int J Oncol*. 2004;24(3):671–678.
21. Shi Y, Han Y, Niu L, Li J, Chen Y. MiR-499 inhibited hypoxia/reoxygenation induced cardiomyocytes injury by targeting SOX6. *Biotechnol Lett*. 2019;41(6–7):837–847.
22. Zhou Z, Wan J, Hou X, Geng J, Li X, Bai X. MicroRNA-27a promotes podocyte injury via PPAR γ -mediated β -catenin activation in diabetic nephropathy. *Cell Death Dis*. 2017;8(3):e2658.
23. Shi M, Tian P, Liu Z, et al. MicroRNA-27a targets Sfrp1 to induce renal fibrosis in diabetic nephropathy by activating Wnt/ β -Catenin signalling. *Biosci Rep*. 2020;40(6).
24. Zhou L, Chen X, Lu M, et al. Wnt/ β -catenin links oxidative stress to podocyte injury and proteinuria. *Kidney Int*. 2019;95(4):830–845.
25. Zhou L, Liu Y. Wnt/ β -catenin signalling and podocyte dysfunction in proteinuric kidney disease. *Nat Rev Nephrol*. 2015;11(9):535–545.
26. Aoki K, Taketo MM. Adenomatous polyposis coli (APC): a multi-functional tumor suppressor gene. *J Cell Sci*. 2007;120(Pt 19):3327–3335.
27. Hankey W, Frankel WL, Groden J. Functions of the APC tumor suppressor protein dependent and independent of canonical WNT signaling: implications for therapeutic targeting. *Canc Metastasis Rev*. 2018;37(1):159–172.
28. Zeng J, Li D, Li Z, Zhang J, Zhao X. Dendrobium officinale attenuates myocardial fibrosis via inhibiting EMT signaling pathway in HFD/STZ-induced diabetic mice. *Biol Pharm Bull*. 2020;43(5):864–872.
29. Kim Y, Lee H, Kim SY, Lim Y. Effects of *lespedeza bicolor* extract on regulation of AMPK associated hepatic lipid metabolism in type 2 diabetic mice. *Antioxidants*. 2019;8(12).
30. Brosius 3rd FC, Alpers CE, Bottinger EP, et al. Mouse models of diabetic nephropathy. *J Am Soc Nephrol : JASN (J Am Soc Nephrol)*. 2009;20(12):2503–2512.
31. An X, Zhang L, Yuan Y, et al. Hyperoside pre-treatment prevents glomerular basement membrane damage in diabetic nephropathy by inhibiting podocyte heparanase expression. *Sci Rep*. 2017;7(1):6413.
32. Rocca CJ, Ur SN, Harrison F, Cherqui S. rAAV9 combined with renal vein injection is optimal for kidney-targeted gene delivery: conclusion of a comparative study. *Gene Ther*. 2014;21(6):618–628.
33. Zhu X, Zhang C, Fan Q, et al. Inhibiting MicroRNA-503 and MicroRNA-181d with losartan ameliorates diabetic nephropathy in KKAY mice. *Med Sci Mon Int Med J Exp Clin Res : Int Med J Exp Clin Res*. 2016;22:3902–3909.
34. Kim H, Dusabimana T, Kim SR, et al. Supplementaion of *Abelmoschus manihot* ameliorates diabetic nephropathy and hepatic steatosis by activating autophagy in mice. *Nutrients*. 2018;10(11).
35. Vallon V, Platt KA, Cunard R, et al. SGLT2 mediates glucose reabsorption in the early proximal tubule. *J Am Soc Nephrol : JASN (J Am Soc Nephrol)*. 2011;22(1):104–112.
36. Pill J, Kraenzlin B, Jander J, et al. Fluorescein-labeled sinistrin as marker of glomerular filtration rate. *Eur J Med Chem*. 2005;40(10):1056–1061.
37. Vallon V, Gerasimova M, Rose MA, et al. SGLT2 inhibitor empagliflozin reduces renal growth and albuminuria in proportion to hyperglycemia and prevents glomerular hyperfiltration in diabetic Akita mice. *Am J Physiol Ren Physiol*. 2014;306(2):F194–F204.
38. Putta S, Lanting L, Sun G, Lawson G, Kato M, Natarajan R. Inhibiting microRNA-192 ameliorates renal fibrosis in diabetic nephropathy. *J Am Soc Nephrol : JASN (J Am Soc Nephrol)*. 2012;23(3):458–469.
39. Chao CS, Tsai CS, Chang YP, Chen JM, Chin HK, Yang SC. Hyperin inhibits nuclear factor kappa B and activates nuclear factor E2-related factor-2 signaling pathways in cisplatin-induced acute kidney injury in mice. *Int Immunopharm*. 2016;40:517–523.
40. Chunzhi G, Zunfeng L, Chengwei Q, Xiangmei B, Jingui Y. Hyperin protects against LPS-induced acute kidney injury by inhibiting TLR4 and NLRP3 signaling pathways. *Oncotarget*. 2016;7(50):82602–82608.
41. Donnapee S, Li J, Yang X, et al. *Cuscuta chinensis* Lam.: a systematic review on ethnopharmacology, phytochemistry and pharmacology of an important traditional herbal medicine. *J Ethnopharmacol*. 2014;157:292–308.
42. Tervaeert TW, Mooyaart AL, Amann K, et al. Pathologic classification of diabetic nephropathy. *J Am Soc Nephrol : JASN (J Am Soc Nephrol)*. 2010;21(4):556–563.
43. Schena FP, Gesualdo L. Pathogenetic mechanisms of diabetic nephropathy. *J Am Soc Nephrol : JASN (J Am Soc Nephrol)*. 2005;16(Suppl 1):S30–S33.
44. Brenneman J, Hill J, Pullen S. Emerging therapeutics for the treatment of diabetic nephropathy. *Bioorg Med Chem Lett*. 2016;26(18):4394–4402.
45. Kishore L, Kaur N, Singh R. Distinct biomarkers for early diagnosis of diabetic nephropathy. *Curr Diabetes Rev*. 2017;13(6):598–605.
46. Yang H, Xie T, Li D, et al. Tim-3 aggravates podocyte injury in diabetic nephropathy by promoting macrophage activation via the NF-kappaB/TNF-alpha pathway. *Mol Metab*. 2019;23:24–36.
47. Arora MK, Sarup Y, Tomar R, Singh M, Kumar P. Amelioration of diabetes-induced diabetic nephropathy by aloe vera: implication of oxidative stress and hyperlipidemia. *J Diet Suppl*. 2019;16(2):227–244.
48. Garofalo C, Borrelli S, Liberti ME, et al. SGLT2 inhibitors: nephroprotective efficacy and side effects. *Medicina (Kaunas)*. 2019;55(6).
49. Sloan LA. Review of glucagon-like peptide-1 receptor agonists for the treatment of type 2 diabetes mellitus in patients with chronic kidney disease and their renal effects. *J Diabetes*. 2019;11(12):938–948.
50. Zhang Y, Wang M, Dong H, Yu X, Zhang J. Anti-hyperglycemic and hepatocyte-protective effects of hyperoside from *Zanthoxylum bungeanum* leaves in mice with high-carbohydrate/high-fat diet and alloxan-induced diabetes. *Int J Mol Med*. 2018;41(1):77–86.
51. Liu B, Tu Y, He W, et al. Hyperoside attenuates renal aging and injury induced by D-galactose via inhibiting AMPK-ULK1 signaling-mediated autophagy. *Ageing*. 2018;10(12):4197–4212.
52. Zhang J, Fu H, Xu Y, Niu Y, An X. Hyperoside reduces albuminuria in diabetic nephropathy at the early stage through ameliorating renal damage and podocyte injury. *J Nat Med*. 2016;70(4):740–748.
53. Zhang L, Dai Q, Hu L, et al. Hyperoside alleviates high glucose-induced proliferation of mesangial cells through the inhibition of the ERK/CREB/miRNA-34a signaling pathway. *Int J Endocrinol*. 2020;2020:1361924.
54. Wang L, Zhang N, Pan HP, Wang Z, Cao ZY. MiR-499-5p contributes to hepatic insulin resistance by suppressing PTEN. *Cell Physiol Biochem : Int J Exp Cell Physiol biochem pharmacol*. 2015;36(6):2357–2365.
55. Fluit MB, Kumari N, Nunlee-Bland G, Nekhai S, Gambhir KK. miRNA-15a, miRNA-15b, and miRNA-499 are reduced in erythrocytes of pre-diabetic african-American adults. *J Diabetes Endocrinol*. 2016;2(1).
56. Ciccacci C, Latini A, Greco C, et al. Association between a MIR499A polymorphism and diabetic neuropathy in type 2 diabetes. *J Diabetes Complicat*. 2018;32(1):11–17.
57. Fawzy MS, Abu AlSel BT, Al Ageeli E, Al-Qahtani SA, Abdel-Daim MM, Toraih EA. Long non-coding RNA MALAT1 and microRNA-499a expression profiles in diabetic ESRD patients undergoing dialysis: a preliminary cross-sectional analysis. *Arch Physiol Biochem*. 2020;126(2):172–182.
58. Zhang K, Sun W, Zhang L, Xu X, Wang J, Hong Y. miR-499 ameliorates podocyte injury by targeting calcineurin in minimal change disease. *Am J Nephrol*. 2018;47(2):94–102.
59. Liu H, Wang T, Chen X, et al. Inhibition of miR-499-5p expression improves nonalcoholic fatty liver disease. *Ann Hum Genet*. 2020, ahg.12374.
60. Calore M, Lorenzon A, Vitiello L, et al. A novel murine model for arrhythmogenic cardiomyopathy points to a pathogenic role of Wnt signalling and miRNA dysregulation. *Cardiovasc Res*. 2019;115(4):739–751.
61. Zhang LL, Liu JJ, Liu F, et al. MiR-499 induces cardiac differentiation of rat mesenchymal stem cells through wnt/ β -catenin signaling pathway. *Biochem Biophys Res Commun*. 2012;420(4):875–881.